

Concept Embeddings for Fuzzy Logic Verification of Deep Neural Networks in Perception Tasks

Gesina Schwalbe
Continental AG

gesina.schwalbe@conti.de

Christian Wirth
Continental AG

christian.2.wirth@continental-corporation.com

Ute Schmid
University of Bamberg
ute.schmid@uni-bamberg.de

Abstract

One major drawback of deep neural networks (DNNs) for use in sensitive application domains is their black-box nature. This makes it hard to verify or monitor complex, symbolic requirements. In this work, we present a simple, yet effective, approach to verify whether a trained convolutional neural network (CNN) respects specified symbolic background knowledge. The knowledge may consist of any fuzzy predicate logic rules. For this, we utilize methods from explainable artificial intelligence (XAI): First, using concept embedding analysis, the output of a computer vision CNN is post-hoc enriched by concept outputs; second, logical rules from prior knowledge are fuzzified to serve as continuous-valued functions on the concept outputs. These can be evaluated with little computational overhead. We demonstrate three diverse use-cases of our method on state-of-the-art object detectors: Finding corner cases, utilizing the rules for detecting and localizing DNN misbehavior during runtime, and comparing the logical consistency of DNNs. The latter is used to find related differences between EfficientDet D1 and Mask R-CNN object detectors. We show that this approach benefits from fuzziness and calibrating the concept outputs.

1. Introduction

Debugging of DNNs or use-cases in safety critical domains like perception tasks in the context of automated driving require verification of semantic prior domain knowledge [32]. Such knowledge can be, e.g., physical laws or typical anatomical structures, and is potentially complex and fuzzy [24]. When using standard object detection CNNs for computer vision tasks [20], it is often hard to formulate such prior knowledge as verifiable constraints, because

there is no mapping of semantic concepts to inputs or (intermediate) outputs: (1) the input is non-symbolic, (2) the semantics of the final output are usually shallow to reduce labeling effort (e.g., few object classes, no sub-objects or other object properties), and (3) standard CNNs are black-box algorithms without an inherent access to encoded semantic concepts (e.g. sub-objects). One way to extract further concept information from a trained CNN is concept (embedding) analysis [4, 8, 13]. The idea is to attach cheap and small models to the CNN intermediate outputs. These are trained to predict the existence of a concept. This also works for large object detectors as shown in [31], requires only few additional labels [8, 12], and leaves the original DNN unchanged.

Concept analysis enriches the detector outputs. Thus, it allows to formulate prior knowledge like “Limbs usually belong to a person” as (fuzzy) predicate logic rules on the extended outputs. The local fulfillment of a rule may be measured as pixel- or region-wise truth values, the *logical consistency scores*. These open up several debugging and verification use-cases: (1) offline identification of *corner cases* (examples with low score) and associated failure modes, (2) self-supervised *monitoring* of logical consistency as error indicator for a CNN during runtime, and (3) comparison of different CNNs e.g. using an aggregated *global logical consistency score*.

Based on concept analysis and t-norm fuzzy logic [24], this work constitutes the following contributions towards the introduced verification use-cases:

- (i) A novel, simple, extensible and scalable framework to construct a *truth value monitor* for logical constraints on task-related semantic concepts (Sec. 3, cf. Fig. 1),
- (ii) Demonstration for pedestrian detection on two *state-of-the-art object detectors* and a safety relevant occlusion robustness rule (Sec. 3.1.3),
- (iii) Evaluation of the framework to *uncover a substantial*

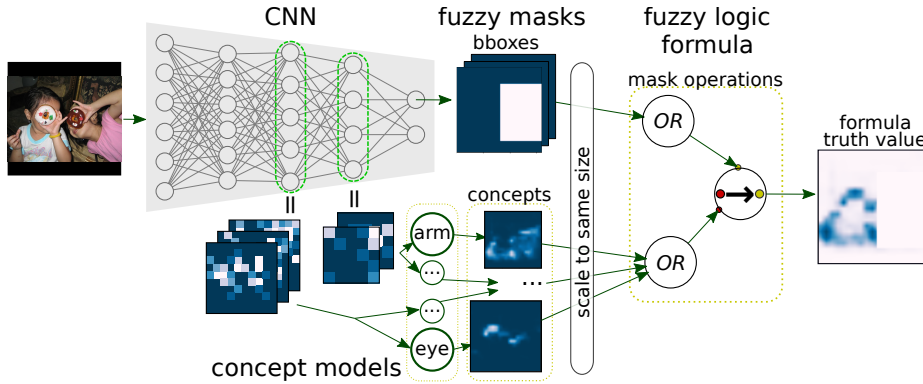


Figure 1. Visualization of our approach from Sec. 3 for the pixel-wise formula $(I_{S_{eye}}(p) \vee I_{S_{arm}}(p) \vee \dots) \rightarrow I_{S_{person}}(p)$. (Image attribution in Fig. 2).

proportion of detection errors with a single rule,

- (iv) Comparison of *options for formulating the monitor*, including different fuzzification methods (Sec. 4.2.1),
- (v) Benefits of model calibration and fuzziness.

2. Related Work

Fuzzy Logic Integration into DNNs: Diligenti *et al.* [6] suggested to use fuzzy logic rules as loss functions for DNN training, relying on continuous t-norm fuzzy logic [24]. This inclusion of semantic prior knowledge to the training was shown to bring significant performance improvements for different types of rules [3, 23, 30], and was extended to several frameworks [3, 22]. While we build upon this idea, the prior work requires all referenced concepts to be part of the DNN output, and does not guarantee that classifier outputs are calibrated.

Concept Embedding Analysis: Bau *et al.* [4] associated activation of single filters to concepts. This was extended by associating concepts to linear combinations (*concept activation vectors*) of neurons [13] or CNN filters [8]. For this, small linear *concept models* are attached to CNN intermediate outputs. We use the successor [31], a post-hoc supervised method, but calibrate the concept outputs to ensure they can be interpreted as truth values. Prior work proposes two semantic consistency metrics based on concept analysis: correct similarity between concept encodings [8, 31], and attribution of early-layer concepts to later-layer ones [13, 34]. Both are restricted in the complexity of verifiable relations, whereas this work can deal with general predicate logic rules.

Calibration: For obtaining calibrated confidence estimates, we use model calibration (cf. Sec. 3.3). Common post-calibration methods [10] are computationally cheap, but approximate Bayesian learning is usually outperforming these methods [16]. However, common variational inference methods [15] are mostly restricted to a mean field approximation, disregarding the covariance, due to computational cost. Therefore, we use a full covariance Laplace

approximation [17], as this is computationally viable with our approach. For a more comprehensive overview, see [1].

Other Monitoring Approaches: Self-supervised runtime monitoring of DNNs usually relies on uncertainty estimation, like [29], or checks of logical consistency with respect to pixel-attribution or costly additional validation inputs, e.g. LiDAR for depth estimation. Uncertainty can detect outliers or proximity to decision boundaries, but no logical inconsistencies. Pixel-attribution can be used to check for spurious input attribution patterns of the model, like (adversarial) outliers [9, 18] or attention not local to detected objects [5]. While this is useful for manual inspection, attention methods are restricted in the rules that can be checked, and our method requires only a single forward pass other than backpropagation (e.g. [2]) or perturbation sampling (e.g. [25, 28]) methods.

3. Approach

Assume one wants to verify that an object detector respects the rule “Heads and limbs belong to a person”. This rule can be formally written as the predicate logic formula

$$\begin{aligned} \forall p \in P: (I_{S_{head}}(p) \vee I_{S_{limb}}(p)) \\ \rightarrow (\exists q \in P: I_{S_{person}}(q) \wedge \text{CloseBy}(p, q)). \end{aligned} \quad (1)$$

for P the domain of pixels in a image. Such a formula with free variables (in our case: the pixel position or image) can be viewed as a function on the variable values that outputs a single truth value for “Is the rule fulfilled”. It can be modeled as computational tree with the nodes being functions and logical operations, i.e. logical conjunctions \vee, \wedge, \neg ; quantifiers \forall, \exists ; and predicates like $I_{S_{person}}$. The main idea for verifying a rule on CNN outputs is to interpret the CNN as family of predicates. This gives the following pipeline (cf. Fig. 1) to evaluate the truth of the rule for given values of the variables:

1. **Obtain outputs of functions** and calibrated (Sec. 3.3) **predicates:**

- Per-pixel values of predicates describing the CNN output, like I_{Sperson} , are derived from the CNN output.
- Values describing internal knowledge of the CNN, like I_{Sarm} , are extracted from the activation maps via concept analysis (Sec. 3.2).

2. Evaluate the residual computational tree of the formula to obtain a final (fuzzy) truth value.

To leverage the knowledge encoded in the confidences of the DNN outputs, we also consider to *fuzzify* all logical operations, i.e. replace them by functions that operate on continuous truth values in $[0, 1]$ (Sec. 3.1). The fuzzy truth value output of a formula may be interpreted as score for the *logical consistency* with that formula. It should be noted that all components (additional concept outputs, calibration, rule evaluation) only require few standard tensor operations, and thus produce negligible computational overhead.

3.1. Fuzzy Logic on DNN Outputs

For fuzzification of logical operations, we rely on the theory of t-norm fuzzy logic [24]. The needed basics thereof are recapitulated in Sec. 3.1.1. Further modeling aspects for fuzzy rules are detailed in Sec. 3.1.2, and applications in Sec. 3.1.3.

3.1.1 Basics of Fuzzy Logic

Fuzzy logic generalizes predicate logic by allowing more than two truth values. Computational nodes of formulas that can be fuzzified are the logical operations. These are:

Logical connectives *NOT* (\neg), *AND* (\wedge), *OR* (\vee), and *implication* (\rightarrow) reduce truth values to a single truth value.

Quantifiers *all* (\forall), and *exists* (\exists) reduce a given domain of values (e.g. pixel positions) to a single truth value using a body formula.

Predicates take symbol values (instantiated variables or constants), and return a single truth value.

For example, predicates arising from DNN confidence outputs are inherently fuzzy. Intuitive fuzzy logical connectives may be defined using a t-norm fuzzy logic [24]. The t-norm fuzzy logics from Tab. 1 represent a generating basis of all t-norm logics with continuous *AND* [24, sec. 2.3.1, p. 48]. Quantifiers can either be naturally expressed via the chosen logical connectives by $(\forall x \in X: F(x)) := (\bigwedge_{x \in X} F(x))$ and $(\exists x \in X: F(x)) := (\bigvee_{x \in X} F(x))$, or be implemented by a mean operation, as suggested in [7]. *Notation:* Predicates with binary output are underlined.

3.1.2 Formulation of Rules for Object Detection

Object detection is subject to several fuzzy logic rules that are based e.g. on laws, physical constraints, or statistical prior knowledge like typical anatomy. Simple examples are:

- Spatial rules, e.g. “Road users usually do not fly.”, or “A person located on top of a bike is usually a cyclist.”
- Hierarchical rules, e.g. “Cars usually have wheels.”, or the example rule from Eq. (1) “Body parts usually belong to a person”.

The last one, e.g., describes a safety relevant occlusion robustness: Infringements of the rule may indicate that the detector can fail in cases of high occlusion when only few body parts are visible (e.g. person behind parked cars). To leverage pixel-wise information obtained from the DNN, we propose a pixel-wise formulation of the example rule. Eq. (1) then translates to $\forall p \in P: F(p)$ for the formula body F

$$I_{\text{IsBodyPart}}(p) \rightarrow I_{\text{IsPartOfAPerson}}(p) \quad (2)$$

with the predicates producing pixel masks of truth values

$$I_{\text{IsPartOfAPerson}}(p) := (\exists q \in P: I_{\text{Sperson}}(q) \wedge \text{CloseBy}(p, q)) \quad (3)$$

$$I_{\text{IsBodyPart}}(p) := \bigvee_{b \in \text{BodyParts}} I_{\text{Sb}}(p) \quad (4)$$

for the domain P of pixels (i.e. pixel coordinates) in a given image, and some pre-defined BodyParts predicates I_{Sb} for $b \in \text{BodyParts}$. This allows to model the logical operations via few standard tensor operations on the mask tensors. Our modeling approach is detailed in the following.

Fuzzy connectives: We consider the three t-norm fuzzy logics detailed in Tab. 1. Note that the non-continuous R-implication $a \rightarrow_R b$ of product and Goedel logic is instable [3] for p where truth values of both a and b are small. To apply the non-fuzzy baseline from Tab. 1, inputs to all logical connectives must be binarized, e.g. at a threshold t_{Bool} (default 0.5). This may reduce memory consumption, but discards potentially valuable confidence information.

Fuzzy quantifiers: The mean as \forall quantifier was suggested in [7] as an intuitive and differentiable implementation. Other than \forall quantifiers derived from a fuzzy *OR*, the $\forall := \text{mean}$ gives rise to the following inequality for a subset $Q \subset P$ and t-norm fuzzy implication:

$$(\forall p \in Q: F(p)) \neq (\forall p \in P: (p \in Q) \rightarrow F(p)) \quad (5)$$

The right hand formulation produces generally large values for small Q ¹. Thus, to keep intuition intact, we recommend the left hand formulation from (5) where applicable. When choosing the \exists quantifier, it must be noted that for $\forall = \text{mean}$ the standard definition $(\exists x: F(x)) = (\neg \forall x: \neg F(x))$ for a formula body F would produce $\exists = \text{mean}$. This ignores high truth values when their proportion in the domain is too low. Thus, a \exists defined from a fuzzy logic \wedge is preferable.

¹ $(\forall p \in P: (p \in Q) \rightarrow F(p)) = \frac{\#P - \#Q}{\#P} + \frac{\#Q}{\#P} \text{mean}_{p \in Q} F(p)$

Logic (abbr.)	Negation $\neg a$	Conjunction $a \wedge b$	Disjunction $a \vee b$	R-Implication $a \rightarrow_R b$	S-Implication $(\neg a) \vee b$
Łukasiewicz (Ł)	$1 - a$	$\max(0, a + b - 1)$	$\min(1, a + b)$	$\min(1, 1 - a + b)$	$\min(1, 1 - a + b)$
Goedel/Minimum (G)	$1 - a$	$\min(a, b)$	$\max(a, b)$	1 if $a \leq b$ else b	$\max(1 - a, b)$
Product/Goguen (P)	$1 - a$	$a \cdot b$	$a + b - a \cdot b$	$\min(1, \frac{b}{a})$	$1 - a + a \cdot b$
Non-fuzzy (Bool)	$\neg(a \geq \tau)$	$(a \geq \tau) \wedge (b \geq \tau)$	$(a \geq \tau) \vee (b \geq \tau)$	$(a < \tau) \vee (b \geq \tau)$	$(a < \tau) \vee (b \geq \tau)$

Table 1. The fuzzy connectives *AND* (*t-norm*), *OR* (*t-conorm*), *residuated implication* (R-implication) and *strong implication* (S-implication) defined by different standard t-norm fuzzy logics. The given non-fuzzy baseline applies the standard Boolean operations \neg, \wedge, \vee to values binarized at a threshold τ_{Bool} (default: 0.5).

Predicates: Typical predicates occurring in rules for object detection are unary concept predicates (“Does the concept apply to the location/region?”) and spatial relations. Using examples from Eq. (2), we demonstrate the different ways to model predicates: using predicted or ground truth bounding boxes ($\text{Is}_{\text{person}}, \text{Is}_{\text{GTPerson}}$), using concept segmentation masks ($\text{Is}_{\text{BodyPart}}$), and manually (CloseBy).

$\text{Is}_{\text{person}}, \text{Is}_{\text{GTPerson}}$ Consider the bounding box outputs for the exemplary person class of an object detector. To turn instance-wise bounding boxes into a semantic segmentation mask for $\text{Is}_{\text{person}}$, we suggest the following simplistic transformation: (1) Each bounding box is turned into a mask by setting pixels inside the bounding box to their bounding box score value, and (2) the box masks are combined using pixel-wise logical *OR* of the respective fuzzy logic (cf. Fig. 1). The same procedure can be applied to ground truth bounding boxes, only with constant binary scores (1 for positives, 0 else).

$\text{Is}_{\text{BodyPart}}$ Segmentation outputs (*concept masks*), e.g. from concept analysis (cf. Sec. 3.2), can serve as unary concept predicates. The masks of different concepts may differ in resolution, e.g. those from concept analysis have the resolution of CNN activation maps. To ensure that all output masks have the same size, one can: (a) up-scale masks to the common largest resolution, e.g. bilinearly [31], or (b) downscale masks to the common smallest resolution, e.g. using maxpooling².

CloseBy A fuzzy spatial close-by relation on pixels can be modeled e.g. as a Gaussian radial distance function on pixel coordinates a, b (with a low cut for memory efficiency):

$$\text{CloseBy}_{\sigma, r}(a, b) := \exp(-d(a, b)^2 / (2\sigma^2)) \quad (6)$$

with $d(a, b) := \|a - b\|_2$ if $\|a - b\|_1 \leq r$ for a window half size r , else 0. The relation becomes trivial if $\sigma = 0$, because $\text{CloseBy}_0(a, b) = 1$ if $a \equiv b$ else 0. Then

²Formally, maxpooling on a unary predicate Is_X can be written as $\exists p' \in P' : \text{CloseBy}(p, p') \wedge \text{Is}_X(p')$ for a pixel $p \in P$ on some other resolution P' , and binary $\text{CloseBy}(p, p') = (\|p - p'\|_1 \leq \lfloor \frac{1}{2}(k_{\text{size}} - 1) \rfloor)$ (cf. Eq. (11)).

e.g. holds $\text{Is}_{\text{PartOfAPerson}}(p) \equiv \text{Is}_{\text{person}}(p)$. A non-trivial spatial relation may help to mitigate concept mask resolution problems: Upscaling low resolution concept masks may cause concept regions to become too large. In the example rule, they may “shoot over” the person areas, leading to noisy rule infringements at the boundary of person areas.

3.1.3 Fuzzy Rules for Verification

Assume one is given a logical rule of the form $R(P) = \forall p \in P : F(p)$. The rule body F yields a truth value when given a pixel in an image or image region P like in Eq. (2). For a concrete image, the pixel outputs of F together form a mask with values in $[0, 1]$ that are high where the formula is fulfilled, and low otherwise. R yields for the image a single truth value that can be interpreted as a logical consistency score for this image. We suggest the following use-cases to utilize R and F for verification, given a test set T .

Corner Case Search: A logical consistency score can be evaluated for each image in T . Outliers with especially low truth value indicate samples in which the DNN shows unexpected logically inconsistent behavior. A pre-selection of such outliers can be a starting point for manual analysis.

Global Logical Consistency Score: The local score $R(P)$ of a rule R for an image P can be aggregated to a single truth value over T , i.e. a global consistency score, using $\forall P \in T : R(P)$. The score e.g. allows comparison of different networks trained on the same dataset, or comparison of different training datasets.

Monitoring: The pixel-wise truth scores given by F give rise to several runtime monitoring scenarios. For our example formula Eq. (1), a monitor would have the task to reveal cases of detector false negatives where some body part was found but no person predicted in the end. A monitor that observes whether pixels p have a suspiciously low truth value can be defined as

$$M(p) := \neg F(p) \in [0, 1], \quad (7)$$

outputting a continuous value that allows to define an alarm threshold $M(p) < \tau_{\text{px}}$. This threshold can be understood as an inconsistency bound. The benefit of the pixel-wise approach is that errors can be localized, such that not the complete prediction must be discarded, but a region in the input. This also allows to ignore warnings about image regions not of interest, e.g. regions far off the ego vehicle trajectory in case of a pedestrian detector in a car.

A pixel-wise monitor M can be extended to a *region-wise monitor* for regions P of pixels in an image. A region monitor marks complete regions or images as spurious based on the pixel truth values. A simple definition would be:

$$M_{\text{reg}}^{\text{simple}}(P) := \exists p \in P: M(p) \in [0, 1] . \quad (8)$$

Note that this is equivalent to $\neg R(P)$ if the equality $(\exists x: f(x)) = (\neg \forall x: \neg f(x))$ holds (cf. fuzzy quantifiers in Sec. 3.1.2). The choice of quantifier is important here: Some are sensitive to outliers, i.e. isolated pixel alarms, (e.g. $\exists = \max$ from Goedel logic), or to the ratio between alarm and non-alarm pixels (e.g. mean), or are computationally expensive (e.g. $\exists = \bigvee$ for the probabilistic sum \bigvee from Product logic). To mitigate influence of single pixel alarms we suggest to add a prior on the shape of pixel-monitor peaks:

$$M_{\text{reg}}^{\text{peaks}}(P) := \exists p \in P: \text{NbCond}(p) \quad (9)$$

The neighbor condition $\text{NbCond}(p)$ should down-weight the truth value of a pixel p if none (Eq. (11)) or, alternatively, not all (Eq. (10)) of its neighbors have a high truth value. We suggest the following formulations:

$$\forall q \in P: \text{CloseBy}(p, q) \rightarrow M(q) \quad (10)$$

$$M(p) \wedge (\exists q \in P \setminus \{p\}: \text{CloseBy}(p, q) \wedge M(q)) \quad (11)$$

Formulation Eq. (10) brings out center points of (approximately radial or quadratic) peaks, and exhibits an efficient implementation as follows. In case CloseBy is binary, it defines the binary set membership $(q \in \text{NbH}(p)) := \text{CloseBy}(p, q)$, and Eq. (10) can be reformulated to $\text{NbCond}(p) = (\forall q \in \text{NbH}(p): M(q))$ (cf. Eq. (5)). Define the neighborhood as square window of size k_{size} , i.e. $\text{CloseBy}(p, q) := (\|p - q\|_1 \leq \lfloor \frac{1}{2}(k_{\text{size}} - 1) \rfloor)$. Using Eq. (5) and $\forall = \text{mean}$, the neighborhood condition Eq. (10) then simplifies to a stride 1 average pooling. With $\exists = \max$:

$$M_{\text{reg}}^{\text{peaks}}(P) = \max_{p \in P} \left(\text{AvgPool2D} \left((M(p))_{p \in P} \right) \right) \quad (12)$$

k_{size} is best chosen to cover at least the minimum expected area of an interesting peak. This ensures that $M_{\text{reg}}^{\text{peaks}}(P_1) > M_{\text{reg}}^{\text{peaks}}(P_2)$ if P_1 contains an interesting peak, P_2 not.

3.2. Concept Analysis for Additional DNN Outputs

Standard symbolic object detection outputs usually include only a small set of objects, e.g. person, and no sub-objects or other object attributes allowing for rich semantics. Our goal is to enrich the output of a DNN by those concepts that are necessary to formulate given prior domain knowledge like Eq. (2) as predicate logic rules. This should be done (1) after training the DNN, (2) without changing the DNN, (3) with little additional training and labeling effort, and (4) extensible, i.e. allowing to later add further concepts in case more domain knowledge is collected. Supervised post-hoc concept analysis constitutes a suitable candidate. *Concept (embedding) analysis* (CA) in general aims to associate semantic concepts with elements in the intermediate output of a DNN in a simple way [31]. Standard types of semantic concepts here can be e.g. texture, material, objects, object parts, or image-level concepts like the scene [4]. The intermediate output of a DNN that is usually considered is a complete layer output. To achieve the association, supervised CA methods learn to predict information on the concept of interest, e.g. a binary segmentation mask, from the intermediate output of the DNN.

We here use the concept analysis method suggested in [31], which was shown to work on CNN object detection. The concept models are attached to the output of one CNN layer. Each consists of a 1×1 -convolution, followed for inference by a sigmoid normalization (and potentially up-scaling). This method only introduces minor computational overhead. The output of the concept models are pixel-masks with confidence values in $[0, 1]$, which are trained to match ground truth binary segmentations of the concept.

3.3. Concept Model Calibration

DNN confidence outputs, including our post-hoc attached concept models, may be badly calibrated. This means that the confidence values do not well match the actual probability with which the prediction is correct [10]. When interpreting confidences as fuzzy truth values, bad calibration violates the fundamental assumption that the truth *meaning* monotonously increases with the truth *value*.

Therefore, we employ approximate Bayesian learning, for calibrating our concept model (cf. Sec. 2). We compute a full covariance approximation of the posterior via Laplace approximate [17]. Despite the required Hessian approximation, we still maintain limited computational overhead, as we only apply it to a single layer (cf. Sec. 3.2) with few parameters. This method can be applied without changing or retraining the base model, making it applicable to any pretrained network.

Model	ECE	Pixel-Acc.	sIoU
Mask R-CNN [11]	0.044	0.956	0.810
EfficientDet D1 [33]	0.071	0.929	0.684

Table 2. Statistics of used $\mathcal{I}_{\text{Sperson}}$ predicates

4. Experiments

This section discusses evaluation results for concept model creation (Sec. 4.1) and the three use-cases (Sec. 4.2), as well as the limitations of our approach (Sec. 4.3).

The suggested use-cases of fuzzy logic formulas for verification are tested on the example occlusion robustness rule from Eq. (2), and for the body parts eye, arm, wrist, leg, ankle. The $\mathcal{I}_{\text{Sperson}}$ predicate is derived from person bounding box outputs of the two networks Mask R-CNN [11] (MR) with ResNet50 backbone, and EfficientDet D1 [33] (EffDet). The weights are trained on the MS COCO train2017 dataset [19], and are taken from PyTorch [26] respectively TensorFlow modelzoo [35] (cf. Tab. 2 for statistics). The ground truth segmentation masks for the body part concepts were derived from the MS COCO 2017 [19] keypoint annotations as done in [31]. Concept models were trained and calibrated on the MS COCO train2017 dataset, with a train/validation split of 4:1. Evaluation results both for the concept model performance and the fuzzy logic are collected on the MS COCO val2017 dataset. The performance of $\mathcal{I}_{\text{Sperson}}$ and the concept model segmentations is evaluated as the set intersection over union (sIoU) [8] between the binary ground truth concept masks $(m_i)_i$ and the predicted and upscaled concept masks $(m_i^{\text{pr}})_i$:

$$\text{sIoU}((m_i)_i, (m_i^{\text{pr}})_i) = \frac{\sum_i \sum m_i \cap (m_i^{\text{pr}} > \tau_{\text{sIoU}})}{\sum_i \sum m_i \cup (m_i^{\text{pr}} > 0.5)} \quad (13)$$

Notation: sIoU_b is measured at optimal τ_{sIoU} (determined on a the validation set), sIoU at 0.5.

4.1. Concept Analysis and Calibration

Literature suggests several losses for concept analysis, including balanced Dice loss [27, 31], and a class-balanced binary cross-entropy (bBCE) [8]. We here also consider standard binary cross-entropy (BCE). We compared calibration and performance of these losses in terms of sIoU, expected calibration error (ECE) and maximum calibration error (MCE) [10]. Results (Tab. 3a) show that Laplace-calibrated BCE outperforms all other variants, *given a tuned sIoU threshold*. Interestingly, balanced losses (Dice, bBCE) suffer from substantial miscalibration. This can be partially countered with the Laplace method, but results are still worse. Calibrating the BCE result only shows minor advantages, therefore we re-evaluated the calibration effects for the full approach (cf. Tab. 6). Improvements are still

mostly small, but consistent (cf. Secs. 4.2.1 and 4.2.2). The sIoU performance of the BCE-trained concept models used in later experiments is given in Tab. 3b. Representations of the larger Mask R-CNN model consistently outperform those of EfficientDet D1 (cf. Sec. 4.2.3).

4.2. Logical Consistency Monitor Applications

If not stated otherwise (cf. Sec. 4.2.1), experiments were conducted for the S-implication formulation of the formula from Eq. (2), with trivial CloseBy_σ from Eq. (6), and the arithmetic mean for \forall , and \max for \exists (this is $\bigvee_x F(x)$ in Goedel logic). The Goedel exists quantifier was chosen as it is the most conservative one of those defined by fuzzy logics, i.e. yields the smallest values [24, Lemma 2.19]. This is a desirable property for safety evaluation with the example rule. Concept masks are bilinearly upscaled to ensure comparability amongst CNNs. For non-fuzzy logic (Tab. 1), the concept masks are binarized at the same thresholds as the monitor outputs, i.e. $\tau_{\text{Bool}} = \tau_{\text{px}}, \tau_{\text{reg}}$ for $\tau_{\text{px}}, \tau_{\text{reg}}$ defined below.

A pixel p is a *false negative pixel* ($\mathcal{I}_{\text{SFN}}(p)$), if $\mathcal{I}_{\text{SFN}}(p) \geq \tau_{\text{ped}} = 0.5$ and

$$\mathcal{I}_{\text{SFN}}(p) := \neg \mathcal{I}_{\text{Sperson}}(p) \wedge \mathcal{I}_{\text{SGTperson}}(p) . \quad (14)$$

Since the logical consistency monitor Eq. (2) shall highlight false negatives of the detector, the ground truth definitions are derived from \mathcal{I}_{SFN} as follows.

Pixel-level Monitor M : This may be used to localize errors within images. For evaluation, we binarize the outputs of M (Eq. (7)) at threshold τ_{px} , with \mathcal{I}_{SFN} as ground truth. Note that our formula will only highlight those parts of false negative areas for which the selected body parts were predicted (e.g. not the torso). Hence, pixel-level recall is naturally comparatively low.

Image-level Monitor M_{reg}^{\cdot} : To investigate suitability for finding images with *some* logical inconsistency, we have a look at the region monitor formulations $M_{\text{reg}}^{\text{simple}}$ (Eq. (8)) and $M_{\text{reg}}^{\text{peaks}}$ (Eq. (12)) for complete images as regions. The ground truth $\text{GT}_{\text{reg}}(P)$ for an image P is defined from the pixel \mathcal{I}_{SFN} values using the same formula as for deriving M_{reg}^{\cdot} from M i.e. for $\text{GT}_{\text{reg}}^{\text{simple}}$ using mean, for $\text{GT}_{\text{reg}}^{\text{peaks}}$ using average pooling then mean. For evaluation, the predicted and ground truth image scores are binarized using thresholds τ_{reg} respectively $\tau_{\text{GTreg}} = 0.5$.

In case of the peak monitor, the average pooling kernel size ksize of both $\text{GT}_{\text{reg}}^{\text{peaks}}$ and $M_{\text{reg}}^{\text{peaks}}$ is set to 33 pixels³, which approximately coincides with the typical height of a head in the test data (cf. size statistics in [31]) at acceptable memory consumption. This means, if half of the pixels within

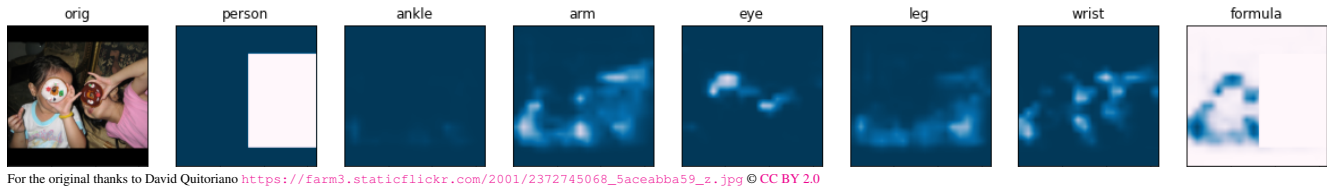
³Preliminary experiments showed: For $\text{ksize} = 2^i + 1, i \leq 5$, differences between ksize for GT_{reg} and M_{reg} only had little influence on the results.

	ECE	MCE	sIoU _b	τ_{sIoU_b}	sIoU	MR		EffDet				
						C	L	sIoU _b	sIoU	L	sIoU _b	sIoU
BCE	0.001 ± 0.000	0.146 ± 0.079	0.297 ± 0.102	0.23 ± 0.06	0.218 ± 0.126							
cal	0.001 ± 0.000	0.140 ± 0.082	0.297 ± 0.102	0.24 ± 0.06	0.218 ± 0.126	ankle	3	0.210	0.132	4	0.142	0.059
Dice	0.010 ± 0.008	0.621 ± 0.082	0.265 ± 0.079	0.59 ± 0.20	0.263 ± 0.081	arm	4	0.330	0.254	6	0.305	0.242
cal	0.001 ± 0.001	0.451 ± 0.121	0.264 ± 0.080	0.52 ± 0.07	0.263 ± 0.080	eye	3	0.436	0.424	5	0.340	0.296
bBCE	0.083 ± 0.047	0.879 ± 0.037	0.115 ± 0.052	0.95 ± 0.00	0.047 ± 0.031	leg	3	0.326	0.264	5	0.310	0.246
cal	0.022 ± 0.012	0.772 ± 0.071	0.228 ± 0.054	0.91 ± 0.05	0.056 ± 0.032	wrist	4	0.184	0.119	6	0.150	0.069

(a) Calibration of Mask R-CNN best concept models (average over concepts)

(b) Performance of used concept models

Table 3. Performance and calibration of the concept models. Tab. 3a: Comparison of calibration and performance of three different concept model losses, with and without calibration, on Mask R-CNN. Tab. 3b: Layer (L) and performance of the used BCE-trained concept models.

For the original thanks to David Quitoriano https://farm3.staticflickr.com/2001/2372745068_5aceabba59_z.jpg © CC BY 2.0Figure 2. Visualization of a EfficientDet D1 corner case for the formula Equation (2), formulated with S-implication, trivial CloseBy , without calibration. *Left to right*: original image, transformed CNN output, predicted concept masks, and pixel-wise formula truth value.

	G	G cal	Ł	Ł cal	P	P cal
MR	0.994	0.994	0.992	0.991	0.992	0.991
EffDet	0.988	0.985	0.981	0.975	0.982	0.977

Table 4. Global logical consistency scores for the simple formula formulation (S-implies, $\sigma = 0$), with and without calibration (cal).

	Bool	Bool cal	Ł	Ł cal	P	P cal
MR	0.829	0.830	0.833	0.833	0.833	0.834
EffDet	0.840	0.843	0.843	0.847	0.843	0.847

Table 5. Pixel level area under ROC curve (AUC) over different pixel binarization thresholds. For abbreviations see Tab. 6.

any 33×33 pixels window are false negatives, the image is marked ground truth faulty. In our setting, 27.7 % of the test images are marked faulty.

4.2.1 Comparing Monitor Formulations

Compared were F1 score, precision, recall and true negative rate of different pixel- (Eq. (7)) and simple image-level (Eq. (8)) monitor formulations at $\tau_{px} = \tau_{reg}^{simple} = 0.5$. Aspects of variation were: fuzzy logics from Tab. 1; standard R-implication versus strong implication; adding calibration; adding denoising of masks, i.e. setting concept mask values < 0.005 to 0; bilinear upscaling versus maxpool downscaling of concept masks; and the trivial $\text{CloseBy}_{\sigma,r}$ from Eq. (6) versus (only for upscaling) the non-trivial

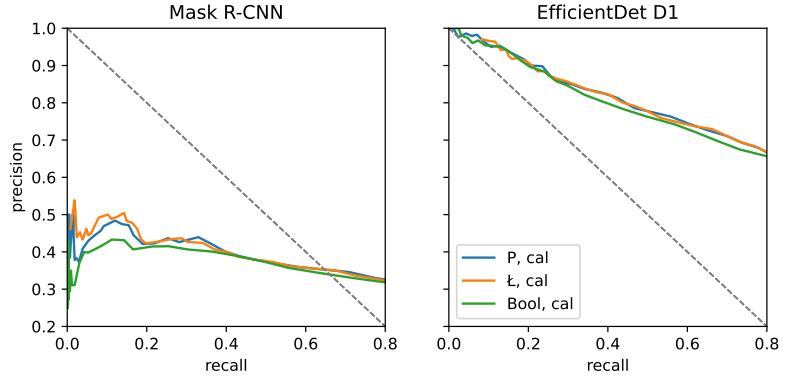
one with $\sigma \approx 2.77$ (truth value of 0.8 at distance of 4px) at $r = 12px$ (window of $25 \times 25px$, cutting at truth values below 0.1). Preliminary experiments showed that R-implication produces many false positives at small input truth values, even with denoising. Slight performance improvements were achieved by: fuzziness; calibration for S-implication; the memory-intense $\text{CloseBy}_{\sigma \neq 0}$ on pixel-level; and downscaling for Łukasiewicz and Product logic, at the cost of truth mask resolution. Therefore, we used the initially described setup for all later experiments.

4.2.2 Self-supervised Error Monitoring Results

Compared were non-fuzzy, Łukasiewicz, and Product logic (cf. Tab. 1), each with and without calibration (cal), both for pixel-level (Eq. (7), Tab. 5) and image-level (Eq. (12), Tab. 6) monitoring. Results show that (1) good error identification performance can be achieved, uncovering a substantial amount of detector errors (cf. contribution (iii)); (2) fuzzy evaluations consistently outperform the non-fuzzy ones (cf. contribution (v)); and (3) calibrated outperform non-calibrated versions (cf. contribution (v)). The image-level results (Tab. 6) further reveal that (4) acceptable precision-recall balances can be achieved for EffDet (e.g. recall of ≥ 0.98 at precision ≥ 0.60 , or precision of ≥ 0.95 at recall ≥ 0.1). This can be seen on the precision-recall curves, as well as on results for F0.1 score (favoring precision) and F10 score (favoring recall) in Tab. 6. Another finding was that (5) the optimal τ_{reg}^{peaks} alarm threshold consistently diverged from the default value 0.5. This suggests that tuning of the threshold on a validation set, similar to τ_{sIoU} , may

	AUC	F1 _{0.5}	$\overline{F1}$	$\overline{F0.1}$	$\overline{F10}$	
Mask R-CNN	Bool	0.619	0.146	0.455	0.421	0.975
	Bool cal	0.620	0.144	0.458	0.423	0.975
	Ł	0.632	0.282	0.462	0.484	0.975
	Ł cal	0.632	0.295	0.461	0.492	0.975
	P	0.632	0.244	0.466	0.467	0.975
	P cal	0.632	0.243	0.465	0.470	0.975
EfficientDet D1	Bool	0.671	0.421	0.749	0.899	0.993
	Bool cal	0.676	0.411	0.749	0.895	0.993
	Ł	0.690	0.557	0.752	0.895	0.993
	Ł cal	0.695	0.592	0.755	0.899	0.993
	P	0.689	0.500	0.751	0.897	0.993
	P cal	0.696	0.523	0.753	0.896	0.993

(a) Summary metrics



(b) Upper left part of precision-recall curves for calibrated formulations

Table 6. Performance comparison of different formula formulations for image-level monitoring. Metrics: area under ROC curve (AUC), F1 at $\tau_{\text{reg}}^{\text{peaks}} = 0.5$, and each $\overline{F1}$, $\overline{F0.1}$, and $\overline{F10}$ for the $\tau_{\text{reg}}^{\text{peaks}}$ yielding the theoretically best corresponding score value.

boost performance values. Without tuning, fuzziness brings a considerable benefit (cf. F1_{0.5} in Tab. 6a). This is especially of interest for cases when threshold tuning is not viable, e.g. because of tuning data availability, or bad generalization of the tuned threshold.

4.2.3 Comparing Logical Consistency of Models

The better performing and calibrated (cf. Tab. 2), and ca. three times larger Mask R-CNN also gives rise to better concept models (Tab. 3b), and achieves the better global logical consistency scores from Sec. 3.1.2 (Sec. 4). This aligns with the findings in Tabs. 5 and 6, where fewer—but still a considerable amount—of the MR false negatives could be recovered using a logical consistency monitor. On the other hand, most errors of the smaller EffDet were recovered using our simple example rule, attesting the model some simple logical gaps. This promises high potential for improvement of EffDet performance on person detection by fine-tuning towards better logical consistency, or by post-processing based on the monitor outputs.

4.2.4 Corner Case Analysis

Finally, we manually inspected the samples with smallest mean pixel-wise logical consistency score⁴. Here, we exclude pixels p regarded trivial (e.g. background), i.e. such with low alarm score $M(p) \leq 10^{-3}$. See Fig. 2 for an example. The analysis revealed for Mask R-CNN: (1) occlusions or strong camera distance deviations that separate body parts from a person can lead to too small bounding boxes, and (2) person features seem to be confused with that of animals and puppets. And (3) EffDet produces false

⁴Precisely, images P_{img} with highest $M_{\text{reg}}^{\text{simple}}(P)$ value from Eq. (8) for the region $P = \{p \in P_{\text{img}} \mid M(p) \geq 10^{-3}\} \subset P_{\text{img}}$.

negatives if the face is only slightly occluded, e.g. by perspective, objects or the image boundary. The found symbolic error modes directly allow to define data augmentation strategies, e.g. adding cases persons segmented by occlusion. To automate corner case selection from new samples, a threshold τ_{reg} for the logical inconsistency score could be fine-tuned on a validation set. Altogether, the fuzzy rule evaluation helps in finding semantic error modes.

4.3. Limitations

The concept model outputs are not guaranteed to well correspond to the originally intended concepts: Bad convergence, a bias in the concept samples, or simply insufficient CNN representations may lead to erroneous concept masks. While symbolic safety properties can be verified, the prior knowledge rules are naturally susceptible to human bias (e.g. anatomical assumptions), potentially leading to unfair safety guarantees. Also, inconsistencies with those pre-defined rules are not guaranteed to accurately correspond to errors. Our approach potentially considerably reduces the amount of test data needed to uncover issues and enable self-supervision, but still inherits all limitations of data based verification methods, like test data representativity. And lastly, our initial modeling approach presented here, e.g. the CNN output transformation, is quite simplistic and may be improved for concrete applications.

5. Conclusion and Outlook

This work presents a simple, yet flexible, self-supervised method to verify and monitor outputs of trained CNNs with respect to logical consistency with symbolic domain knowledge rules. The post-hoc method produces little computational overhead, and leverages the performance benefits of fuzziness and calibration: It allows to identify a consider-

able proportion of detection errors, given proper fine-tuning of the alarm threshold. Furthermore, the used logical consistency scores can help in finding error modes, and to directly compare CNNs. For example, Mask R-CNN comes up with both considerably better representations, and conformity with a simple occlusion robustness rule for person detection, in comparison to EfficientDet D1. Thus, we are looking forward to see results on further models, tasks, and example rules, including investigation of how to model temporal aspects. Also, it should be investigated how much a trained model could be improved by self-supervised fine-tuning via the logical consistency scores.

Acknowledgements

The research leading to these results is partly funded by the German Federal Ministry for Economic Affairs and Energy within the project “Methoden und Maßnahmen zur Absicherung von KI basierten Wahrnehmungsfunktionen für das automatisierte Fahren (KI-Absicherung)”. The authors would like to thank the consortium for the successful cooperation.

References

- [1] Moloud Abdar, Farhad Pourpanah, Sadiq Hussain, Dana Rezazadegan, Li Liu, Mohammad Ghavamzadeh, Paul Fieguth, Xiaochun Cao, Abbas Khosravi, U. Rajendra Acharya, Vladimir Makarek, and Saeid Nahavandi. A review of uncertainty quantification in deep learning: Techniques, applications and challenges. *Information Fusion*, 76:243–297, 2021. [2](#)
- [2] Sebastian Bach, Alexander Binder, Grégoire Montavon, Frederick Klauschen, Klaus-Robert Müller, and Wojciech Samek. On pixel-wise explanations for non-linear classifier decisions by layer-wise relevance propagation. *PLOS ONE*, 10(7):e0130140, July 2015. [2](#)
- [3] Samy Badreddine, Artur d’Avila Garcez, Luciano Serafini, and Michael Spranger. Logic tensor networks. *CoRR*, abs/2012.13635, Jan. 2021. [2](#), [3](#)
- [4] David Bau, Bolei Zhou, Aditya Khosla, Aude Oliva, and Antonio Torralba. Network dissection: Quantifying interpretability of deep visual representations. In *Proc. 2017 IEEE Conf. Comput. Vision and Pattern Recognition*, pages 3319–3327. IEEE Computer Society, 2017. [1](#), [2](#), [5](#)
- [5] Chih-Hong Cheng, Georg Nührenberg, Chung-Hao Huang, Harald Ruess, and Hirotoishi Yasuoka. Towards dependability metrics for neural networks. In *16th ACM/IEEE Int. Conf. Formal Methods and Models for System Design*, pages 43–46. IEEE, 2018. [2](#)
- [6] Michelangelo Diligenti, Marco Gori, and Claudio Saccà. Semantic-based regularization for learning and inference. *Artificial Intelligence*, 244:143–165, Mar. 2017. [2](#)
- [7] Ivan Donadello, Luciano Serafini, and Artur S. d’Avila Garcez. Logic tensor networks for semantic image interpretation. In *Proc. 26th Int. Joint Conf. Artificial Intelligence*, pages 1596–1602. ijcai.org, 2017. [3](#), [12](#), [13](#)
- [8] Ruth Fong and Andrea Vedaldi. Net2Vec: Quantifying and explaining how concepts are encoded by filters in deep neural networks. In *Proc. 2018 IEEE Conf. Comput. Vision and Pattern Recognition*, pages 8730–8738. IEEE Computer Society, 2018. [1](#), [2](#), [6](#)
- [9] Ruth C. Fong and Andrea Vedaldi. Interpretable explanations of black boxes by meaningful perturbation. In *Proc. 2017 IEEE Int. Conf. on Comput. Vision*, pages 3449–3457. IEEE Computer Society, 2017. [2](#)
- [10] Chuan Guo, Geoff Pleiss, Yu Sun, and Kilian Q. Weinberger. On calibration of modern neural networks. In Doina Precup and Yee Whye Teh, editors, *Proceedings of the 34th International Conference on Machine Learning, ICML 2017, Sydney, NSW, Australia, 6-11 August 2017*, volume 70 of *Proceedings of Machine Learning Research*, pages 1321–1330. PMLR, 2017. [2](#), [5](#), [6](#)
- [11] K. He, G. Gkioxari, P. Dollár, and R. Girshick. Mask R-CNN. In *2017 IEEE International Conference on Computer Vision (ICCV)*, pages 2980–2988, Oct. 2017. [6](#)
- [12] Dmitry Kazhdan, Botty Dimanov, Helena Andres Terre, Mateja Jamnik, Pietro Liò, and Adrian Weller. Is disentanglement all you need? comparing concept-based & disentanglement approaches. *arXiv:2104.06917 [cs]*, Apr. 2021. [1](#)
- [13] Been Kim, Martin Wattenberg, Justin Gilmer, Carrie Cai, James Wexler, Fernanda Viegas, and Rory Sayres. Interpretability beyond feature attribution: Quantitative testing with concept activation vectors (TCAV). In *Proc. 35th Int. Conf. Machine Learning*, volume 80 of *Proceedings of Machine Learning Research*, pages 2668–2677. PMLR, July 2018. [1](#), [2](#)
- [14] Diederik P. Kingma and Jimmy Ba. Adam: A method for stochastic optimization. In *Proc. 3rd Int. Conf. Learning Representations*, 2015. [11](#)
- [15] Durk P Kingma, Tim Salimans, and Max Welling. Variational dropout and the local reparameterization trick. In C. Cortes, N. Lawrence, D. Lee, M. Sugiyama, and R. Garnett, editors, *Advances in Neural Information Processing Systems*, volume 28. Curran Associates, Inc., 2015. [2](#)
- [16] Ranganath Krishnan and Omesh Tickoo. Improving model calibration with accuracy versus uncertainty optimization. In Hugo Larochelle, Marc’Aurelio Ranzato, Raia Hadsell, Maria-Florina Balcan, and Hsuan-Tien Lin, editors, *Advances in Neural Information Processing Systems 33: Annual Conference on Neural Information Processing Systems 2020, NeurIPS 2020, December 6-12, 2020, virtual*, 2020. [2](#)
- [17] Agustinus Kristiadi, Matthias Hein, and Philipp Hennig. Being bayesian, even just a bit, fixes overconfidence in relu networks. In *Proceedings of the 37th International Conference on Machine Learning, ICML 2020, 13-18 July 2020, Virtual Event*, volume 119 of *Proceedings of Machine Learning Research*, pages 5436–5446. PMLR, 2020. [2](#), [5](#)
- [18] Sebastian Lapuschkin, Stephan Wäldchen, Alexander Binder, Grégoire Montavon, Wojciech Samek, and Klaus-Robert Müller. Unmasking Clever Hans predictors and assessing what machines really learn. *Nature Communications*, 10(1):1096, Mar. 2019. [2](#)

- [19] Tsung-Yi Lin, Michael Maire, Serge J. Belongie, James Hays, Pietro Perona, Deva Ramanan, Piotr Dollár, and C. Lawrence Zitnick. Microsoft COCO: Common objects in context. In *Proc. 13th European Conf. Computer Vision - Part V*, volume 8693 of *Lecture Notes in Computer Science*, pages 740–755. Springer International Publishing, 2014. 6, 11
- [20] Li Liu, Wanli Ouyang, Xiaogang Wang, Paul Fieguth, Jie Chen, Xinwang Liu, and Matti Pietikäinen. Deep learning for generic object detection: A survey. *International Journal of Computer Vision*, 128(2):261–318, Feb. 2020. 1
- [21] David J. C. MacKay. The evidence framework applied to classification networks. *Neural Comput.*, 4(5):720–736, 1992. 11
- [22] Giuseppe Marra, Francesco Giannini, Michelangelo Diligenti, and Marco Gori. LYRICS: A general interface layer to integrate logic inference and deep learning. In *Proc. European Conf. Machine Learning and Principles of Knowledge Discovery 2019*, Sept. 2019. 2
- [23] Yatin Nandwani, Abhishek Pathak, Mausam, and Parag Singla. A primal dual formulation for deep learning with constraints. In *Advances in Neural Information Processing Systems 32*, pages 12157–12168. Curran Associates, Inc., 2019. 2
- [24] Vilém Novák, Irina Perfilieva, and J. Mockor. *Mathematical Principles of Fuzzy Logic*. The Springer International Series in Engineering and Computer Science. Springer US, Jan. 1999. 1, 2, 3, 6
- [25] Vitali Petsiuk, Rajiv Jain, Varun Manjunatha, Vlad I. Morariu, Ashutosh Mehra, Vicente Ordonez, and Kate Saenko. Black-box explanation of object detectors via saliency maps. *arXiv:2006.03204 [cs]*, June 2020. 2
- [26] pytorch. Torchvision. <https://github.com/pytorch/vision/v0.10.0>, Oct. 2021. 6
- [27] Johannes Rabold, Gesina Schwalbe, and Ute Schmid. Expressive explanations of DNNs by combining concept analysis with ILP. In *KI 2020: Advances in Artificial Intelligence*, Lecture Notes in Computer Science, pages 148–162. Springer International Publishing, 2020. 6
- [28] Marco Túlio Ribeiro, Sameer Singh, and Carlos Guestrin. "Why should I trust you?": Explaining the predictions of any classifier. In *Proc. 22nd ACM SIGKDD Int. Conf. Knowledge Discovery and Data Mining*, KDD '16, pages 1135–1144. ACM, 2016. 2
- [29] Matthias Rottmann, Pascal Colling, Thomas Paul Hack, Robin Chan, Fabian Hüger, Peter Schlicht, and Hanno Gottschalk. Prediction error meta classification in semantic segmentation: Detection via aggregated dispersion measures of softmax probabilities. In *Proc. 2020 Int. Joint Conf. Neural Networks*, pages 1–9, July 2020. 2
- [30] Soumali Roychowdhury, Michelangelo Diligenti, and Marco Gori. Image classification using deep learning and prior knowledge. In *Workshops of the 32nd AAAI Conf. Artificial Intelligence*, volume WS-18 of *AAAI Workshops*, pages 336–343. AAAI Press, June 2018. 2
- [31] Gesina Schwalbe. Verification of size invariance in DNN activations using concept embeddings. In *Artificial Intelligence Applications and Innovations*, IFIP Advances in Information and Communication Technology, pages 374–386. Springer International Publishing, 2021. 1, 2, 4, 5, 6, 11
- [32] Gesina Schwalbe and Martin Schels. A survey on methods for the safety assurance of machine learning based systems. In *Proc. 10th European Congress Embedded Real Time Software and Systems*, Jan. 2020. 1
- [33] Mingxing Tan, Ruoming Pang, and Quoc V. Le. Efficient-Det: Scalable and efficient object detection. In *Proc. 2020 IEEE/CVF Conf. Comput. Vision and Pattern Recognition*, pages 10781–10790, 2020. 6
- [34] Dan Wang, Xinrui Cui, and Z. Jane Wang. CHAIN: Concept-harmonized hierarchical inference interpretation of deep convolutional neural networks. *CoRR*, abs/2002.01660, 2020. 2
- [35] Ross Wightman. EfficientDet (PyTorch). <https://github.com/rwightman/efficientdet-pytorch/tree/75e16c2f>, Oct. 2021. 6

Appendix Overview

This supplemental material collects additional results and details for the experiments described in the main paper. Specifically, it gives further evidence for the following claims made in the main paper:

- Appendix **B**: *The main formula used in the main paper can be implemented as parallelizable windowed operation* under some modeling constraints.
- Appendix **C**: This section gives detailed results of the preliminary experiments on the comparison of monitor formulations referenced in the main paper. These show that *the simple rule formulation used in the main paper is a valid choice* for the later experiments in the main paper.
- Appendix **D**: *Fuzziness improves the error-detection performance of a logical consistency monitor when the hyperparameter for the binarization threshold cannot be tuned* on a validation set.
- Appendix **E**: For the peak-concentrated image-level monitor formulation, *the kernel size hyperparameter of the monitor can be chosen independently of that of the ground truth*.

Appendix **A** gives details on the chosen hyperparameter values for the experiments to ensure reducibility.

A. Implementation Notes: Hyperparameter Choices

In the following, hyperparameter choices for our experiments are detailed. An overview on further hyperparameters introduced in this supplemental material and the main paper can be found in Tab. 7.

Settings applicable to all experiments are:

- An image size of 400×400 pixels was used for Mask R-CNN, 640×640 pixels for EfficientDet D1.
- Images were first zero-padded to square size, then resized to the desired image size (keeping the aspect ratio).
- For metrics working on binary pixel values, output masks (after transformation of bounding boxes to masks) are thresholded at a value of 0.5.

Concept Data The body part segmentation masks were generated from keypoint annotations as proposed in [31]. Point concepts (eye, wrist, ankle) are added as filled circle of white pixels. Limb concepts (arm, leg) get filled circles at edges and joints, and lines connecting them where skeletal connections exist. The concepts consist of the following keypoints:

- arm: left/right shoulder, elbow, wrist
- leg: left/right hip, knee, ankle
- eye, wrist, ankle: corresponding left/right keypoints

Circle diameter and line width were set to 5% of the estimated person body height in pixels (using estimation algorithm from [31]). The body height defaults to the bounding box height if it cannot be estimated from keypoint links of the annotation. Keypoints annotated as occluded are treated as not present.

Calibration and Formula Evaluations The measurement of calibration and performance metrics on the main CNN, as well as the evaluations of the fuzzy logic formulas, used the following settings:

- Evaluation batch size: 64;
- Data split: All images from the MS COCO dataset [19] val2017 split are used for evaluation.

Concept Model Training The training and evaluation of the concept models used the following settings in accordance with [31]:

- Metric and loss calculation: Concept model outputs (after convolution) are first bilinearly upsampled to match the ground truth resolution, then normalized. For BCE-losses, normalization is skipped and the loss is calculated in logit space.
- Loss for second stage training of the Laplace approximation parameters [21]: binary cross-entropy (in logit space);
- Data split: The training and validation data sets are taken from the MS COCO dataset [19] train2017 split, the test data from the val2017 split. For each concept, only those samples are included that contain any positive concept mask pixel. The train2017 samples for a concept are randomly split into training and validation set, at a ratio of 4:1.
- Optimizer and learning rate: Adam [14] from PyTorch version 1.9.0 implementation, with a learning rate of 0.001, and default beta values of 0.9 and 0.999; no weight decay;
- Batch sizes: 8 for training, 64 for validation, and 6 for the second stage training of the Laplace approximation parameters [21];
- Early stopping: Concept models are trained for at most 7 epochs. Training is stopped early after an epoch if the validation loss decreases less than 0.001 for each in three successive epochs.

Name	Default	Function
t_{sIoU}	0.5	Threshold used to determine the set intersection over union performance
t_{denoise}	0.005	Denoise low values of $\text{IsBodyPart}(\bullet)$ masks
t_{ped}	0.5	Binarizing threshold for $\text{IsPerson}(\bullet)$ masks
t_{px}	0.5	Binarizing threshold for pixel-level monitor output masks
t_{reg}	0.5	Binarizing threshold for image-level monitor outputs
t_{sIoU}	0.5	Binarizing threshold for pixel-level monitor outputs for measuring sIoU
t_{Bool}	0.5	Binarizing threshold for all mask in non-fuzzy logic
k_{size}	33	Width of the quadratic kernel for defining a (binary) pixel neighborhood

Table 7. Overview of hyperparameters and their default values used in the formula calculation (here and in the main paper).

B. Implementation Notes: Parallelization of Example Formula

Consider the mask operation CloseToAb that accepts a mask Q and returns a mask P with each pixel p holding the truth value for “ p is close to a pixel q in Q at which concept b is present”. This is used in the example formula from the main paper as will become clear from Definition 2. This section shows that under some conditions this CloseToAb can be implemented as a windowed operation on the mask Q , similar to a convolution or pooling operation. Furthermore, an upper bound is given for the minimal window size (cf. Proposition 1). The **windowing allows parallelization, and thus a potentially massive speedup**. Note, however, that this may be quite memory intensive, as it is not guaranteed that the operation can be represented as sparse matrix operations.

Before formally defining CloseToAb in Definition 2, some notation for pixel indices is introduced that allows to interpret them as coordinates (with standard distance measures like L_1).

Definition 1. Let h, h', w, w' be natural numbers (mask heights and widths), and let $Q \in [0, 1]^{h' \times w'}$, $P \in [0, 1]^{h \times w}$ be 2D masks. A mask coordinate system here denotes an injective mapping of dimensions (i_h, i_w) in a mask P to pixel positions in 2D space \mathbb{R}^2 . By default map the dimension (i_h, i_w) to the point $(i_h + 0.5, i_w + 0.5)$, i.e. a pixel has a width of 1×1 and pixel coordinates refer to pixel centers. Let $p \in \mathbb{R}^2$ be a pixel position.

- (a) *Pixel positions in a mask:* Denote by $p \in P$ that p is a pixel in the mask P .
- (b) *Pixel values of a mask:* Given that $p \in P$, denote by $P(p)$ the value at the pixel position p in the mask P .
- (c) *Sub-masks of a mask:* A mask $W \in [0, 1]^{h \times w}$ is a window or sub-mask in $P \in [0, 1]^{h' \times w'}$, denoted $W \subset P$, if $h \leq h', w \leq w'$, and there is a mask coordinate system for W and P such that for all pixel positions $p \in W$ holds $p \in P$ and $W(p) = P(p)$.

Definition 2. Let h, h', w, w' be integers and $Q \in [0, 1]^{h' \times w'}$ be a mask. Assume a logic is given with predicates Is_b and CloseBy of arity one respectively two, which both operate on pixel positions. We define the following mask operation:

$$\text{CloseToAb}: [0, 1]^{h' \times w'} \rightarrow [0, 1]^{h \times w} \quad (15)$$

$$P(p) := (\exists q \in Q: \text{Is}_b(q) \wedge \text{CloseBy}(p, q)) \quad (16)$$

for $p \in P := \text{CloseToAb}(Q)$.

This is used in the example formula from the main paper. (Note that P and Q need not have the same resolution.)

The following proposition states that, under some conditions, CloseToAb can be implemented as a windowed operation. And, if the CloseBy predicate becomes zero at some L_1 distance r , the window size of the windowed operation may be chosen $2r + 1$ (or smaller). This means, $2r + 1$ is the maximum window size necessary to ensure an exact implementation.

Proposition 1. Consider a (fuzzy) logic, and $\text{Is}_b, \text{CloseBy}$, and the masks Q and $P = \text{CloseToAb}(Q)$ as in Definition 2. Assume the following:

- (a) \exists is either defined as an arithmetic mean [7], or defined using the logical OR, i.e. for a domain X and a formula f holds $\exists x \in X: f(x) := \bigvee_{x \in X} f(x)$.
- (b) There is a square integer window size $2r + 1$ such that $\text{CloseBy}(p, q) = 0$ if $\|p - q\|_1 > r$ for any pixel positions p, q . This is e.g. the case for the suggested max-pooling or Gaussian CloseBy from the main paper.

Then, $P(p)$ for a pixel position $p \in P$ at most depends on the pixel values in the window $W_p \subset Q$ of size $(2r + 1) \times (2r + 1)$ centered at p , i.e.

$$\text{CloseToAb}(Q)(p) = (\exists q \in W_p: \text{Is}_b(q) \wedge \text{CloseBy}(p, q)) \quad (17)$$

Proof. Let $f(p, q) := \text{Is}_b(q) \wedge \text{CloseBy}(p, q)$. Note that

- (i) $f(p, q) = 0$ if $\text{closeBy}(p, q) = 0$, and
- (ii) $q \in W_p$ if $f(p, q) \neq 0$, because for $q \in Q \setminus W_p$ holds:
 - $\|p - q\|_1 > r$ by definition of the window W_p , thus
 - $\text{closeBy}(p, q) = 0$ by (b), and so
 - $f(p, q) = 0$ by (*).

For \exists defined via logical *OR* according to assumption (a), the formula becomes

$$P(p) = \exists q \in Q: f(p, q) \stackrel{(a)}{=} \bigvee_{q \in Q} f(p, q) \quad (18)$$

$$\stackrel{(i)}{=} 0 \vee \bigvee_{\substack{q \in Q \\ f(p, q) \neq 0}} f(p, q) \stackrel{(ii)}{=} 0 \vee \bigvee_{\substack{q \in W_p \\ f(p, q) \neq 0}} f(p, q) \quad (19)$$

$$\stackrel{(a)}{=} \exists q \in W_p: f(p, q) \quad (20)$$

For \exists defined via arithmetic mean, note that

$$\exists q \in Q: f(p, q) = \frac{1}{\#Q} \sum_{q \in Q} f(p, q). \quad (21)$$

Replacing all occurrences of $\bigvee_{q \in Q}$ with $\frac{1}{\#Q} \sum_{q \in Q}$ in the above calculation finalizes the proof. \square

Remark 1. Note that the notation, Definition 2, and Proposition 1 all can easily be generalized to masks $Q \in [0, 1]^{n_1 \times \dots \times n_d}$ of arbitrary dimension $d \geq 1$, with pixel positions in \mathbb{R}^d . So, the rule formulation and efficient implementation can be applied not only to 2D masks, but also e.g. 3D masks consisting of several channels or frames.

Remark 2. The following special cases further simplify the implementation:

- (a) *Trivial case:* In case $r = 1$, as in the experiments in the main paper, $\text{closeToAb}(Q)(p) = \text{Isb}(p) \wedge \text{closeBy}(p, p)$.

- (b) *Maxpooling case:* For $\exists = \max$ and binary

$$\text{closeBy}(p, q) := (\|p - q\|_1 \leq r) \quad (22)$$

($\text{closeBy}(p, q)$ is one if q lies in a square window around p , else 0) closeToAb becomes a simple maxpooling operation on Q with kernel size $2r + 1$. The stride of the pooling operation is such that the size $h' \times w'$ of Q is reduced to the size $h \times w$ of P . This is used for the downscaling operation which was suggested in the main paper and is further investigated in Appendix C.

- (c) *Convolutional case:* For $\exists = \text{mean}$ [7] and Product logic, closeToAb becomes a simple linear convolution followed by applying a pixel-wise factor $\frac{1}{(h' \cdot w')^2}$. Kernel weights for the kernel window with center p are defined by $\text{closeBy}(p, \cdot)$.

C. Comparison of Monitor Formulations

This section collects further considerations and the results for directly comparing different monitor formulations. The following variations are considered (cf. Tab. 8):

Fuzzy logics from the main paper: Łukasiewicz, Product, and Goedel fuzzy logic; and non-fuzzy predicate logic on concept masks binarized at τ_{Bool} .

Implication style: Sstrong implication (S-implies) or residuated implication (R-implies).

Denoising: With or without setting concept mask values lower than $\tau_{\text{denoise}} = 0.005$ to 0. This can be modeled as pixel-wise operation $(\text{Isb}(p) \geq \tau_{\text{denoise}}) \wedge \text{Isb}(p)$ for pixels p and concept b with concept mask $\text{Isb}(\cdot)$.

Choice of closeBy : Considered are the Gaussian $\text{closeBy}_{\sigma, r}$ from the main paper, different mask scaling options, and trivial $\text{closeBy}_{\sigma=0, r=1}$. The following three settings are compared here:

- bilinear upscaling with trivial closeBy
- bilinear upscaling with non-trivial $\text{closeBy}_{\sigma, r}$, $\sigma \approx 2.77$ and $r = 12\text{px}$ (in visualizations shorted to *CoveredBy*)
- downscaling using maxpooling with trivial closeBy

Calibration: With or without post-hoc Laplace calibration of concept model outputs.

On the Denoising The *denoising* intends to reduce the instable cases of pixels for R-implies. These are the cases where both values of IsBodyPart and IsPerson are very low, but IsBodyPart is larger than IsPerson . For Product and Goedel logic this causes $\text{IsBodyPart}(p) \rightarrow_R \text{IsPerson}(p)$ to jump from 1 to a smaller value (cf. R-implies definitions from the main paper).

On the closeBy Choice Either approach for *implementing closeBy* —the fuzzy but memory-intense Gaussian $\text{closeBy}_{\sigma, r}$, and the non-fuzzy maxpooling based one—has the effect of enlarging the area of positive truth values. This is useful if concept masks have different resolutions and might not match precisely at the boundaries. This leads to low truth values in boundary regions if a low-resolution mask and a higher-resolution mask are scaled and combined in a *AND* or *implies* operation.

Results Results for the following monitor formulations can be found below (both using binarization thresholds $\tau_{\text{px}} = 0.5 = \tau_{\text{reg}}^{\text{simple}}$):

- Pixel-wise monitor M : Fig. 3 for Mask R-CNN, Fig. 4 for EfficientDet D1.
- Image-level monitor $M_{\text{reg}}^{\text{simple}}$: Fig. 5 for Mask R-CNN, Fig. 6 for EfficientDet D1.

Furthermore, global scores for different monitor formulations are compared in Fig. 7. It must be noted that the pixel-level monitor is expected to have low recall: Only such detector false negative pixels should be highlighted that are inconsistent with the considered rule, which can only be those that are part of one of the considered body parts (no torso, bounding box corners, etc.). The following can be seen from the visualizations:

- (1) *Fuzziness*: For S-implication, **non-fuzzy logic performs consistently slightly worse than fuzzy logic.**
- (2) *Implication style and denoising*: Despite denoising, **R-implication is still much too sensitive** and causes many false positives (cf. low true negative rates, and suspiciously high recall on pixel-level).
- (3) *CloseBy*: **Using a non-trivial CloseBy gives slight (downscaling) up to significant (non-trivial CloseBy $_{\sigma,r}$) performance benefits**, as can be seen e.g. from the F1 scores. However, CloseBy $_{\sigma,r}$ either cannot be parallelized or requires lots of memory for the windowed operation, and downscaling significantly reduces (localization) information. Thus, in the main paper only the trivial CloseBy is used, and noise problems smoothed using the neighborhood condition for the image-level monitor (cf. Appendix E).
- (4) *Calibration* on pixel-level seems to have a **negative effect on precision and a positive one on recall, resulting in comparable F1 scores.** On image-level, calibration seems to have the least effect of all aspects of variation on the monitor performance. **For the global scores calibration has the visible effect of decreasing logical consistency for any rule formulation.**
- (5) The comparison of the lack of *global logical consistency* in Fig. 7 shows that **the choice of rule formulation has no influence on the trend of the global consistency.** Any choice of variation attests EfficientDet D1 the clearly worse score.

D. Benefits of Fuzziness without Monitor Threshold Tuning

Fig. 8 shows the F1 scores of the pixel- and the image-level monitors considered in the main paper, plotted by the binarization threshold τ_{px} respectively $\tau_{\text{reg}}^{\text{peaks}}$. Concretely compared are the non-fuzzy baseline with Łukasiewicz and Product t-norm fuzzy logic, with calibrated and non-calibrated concept models. The following can be seen:

- (1) **When deviating from the optimal threshold, fuzzy formulations clearly outperform the non-fuzzy alternative.**
- (2) The optimal thresholds, and corresponding optimal F1 scores on the test set nearly coincide for all formulations.
- (3) In all cases, F1-by-threshold curve has a unique maximum, and the threshold for this optimal F1 score is far from the default of 0.5. This **highlights the potential performance increase by tuning the hyperparameter τ_{px} respectively τ_{reg} .**
- (4) It can be seen a consistent slight performance benefit of calibration.

E. Choice of k_{size} for Image-level Monitor

The peak-concentrated image-level monitor $M_{\text{reg}}^{\text{peaks}}$ used in experiments in the main paper has the additional hyperparameter of the average pooling kernel size k_{size} for the image-level monitor neighborhood condition. As both the monitor $M_{\text{reg}}^{\text{peaks}}$ and $\text{GT}_{\text{reg}}^{\text{peaks}}$ were defined using the neighborhood condition, each has a tunable k_{size} parameter, k_{size_M} and $k_{\text{size}_{\text{GT}}}$.

Ground Truth Positive Rates $k_{\text{size}_{\text{GT}}}$ influences the ground truth positive rate of images in the dataset, as smaller kernel window size values are more sensible to smaller (possibly noisy) peaks. Tab. 9 shows the positive rates for exponentially increasing $k_{\text{size}_{\text{GT}}}$ and two $\tau_{\text{GTreg}}^{\text{peaks}}$ settings. What positive rate is obtained for which k_{size} setting depends on the distribution of alarm area sizes in the test dataset. For example, for $\tau_{\text{GTreg}}^{\text{peaks}}$ the positive rate approximately linearly increases with the kernel size. Note that for $k_{\text{size}_{\text{GT}}}$, this is identical with the ground truth for the simple monitor formulation $M_{\text{reg}}^{\text{simple}}$.

Dependence of Monitor Results on $k_{\text{size}_{\text{GT}}}$ The following results show that larger kernel sizes of the monitor (prediction) bring some benefit, regardless of the ground truth kernel size. Investigated were odd kernel sizes $2^i + 1$, $2 \leq i \leq 5$ and kernel size of 1 as baseline. Here evaluated were the neighborhood (nb) image-level formulation of the monitor from the main paper, for the rule formulation with S-implication and calibration. Compared were different Łukasiewicz and non-fuzzy logic, different kernel sizes k_{size_M} , $k_{\text{size}_{\text{GT}}}$, and binarization thresholds $\tau_{\text{reg}}^{\text{peaks}}$, $\tau_{\text{GTreg}}^{\text{peaks}}$. Results are shown

- for fixed middle sized $k_{\text{size}_{\text{GT}}} = 9$ in Fig. 9,
- for k_{size_M} fixed in Fig. 11,
- for $k_{\text{size}_M} = k_{\text{size}_{\text{GT}}}$ in Fig. 10.

Aspect	Description
Implication	Whether S- or R-implication is used
CloseBy, Scaling	Formulation of the CloseBy: upscaling of small masks with either non- or trivial $\text{CloseBy}_{\sigma,r}$; or max-downscaling of large masks
Calibration	Whether Laplace calibration is applied to the concept models during inference
Denoising	Whether truth values in concept masks $\mathbb{I}_{\text{sb}}(\cdot)$ that are below τ_{denoise} are set to 0

Table 8. Overview on the different aspects of variation tested for the formulation of the formula from the main paper (cf. Appendix C)

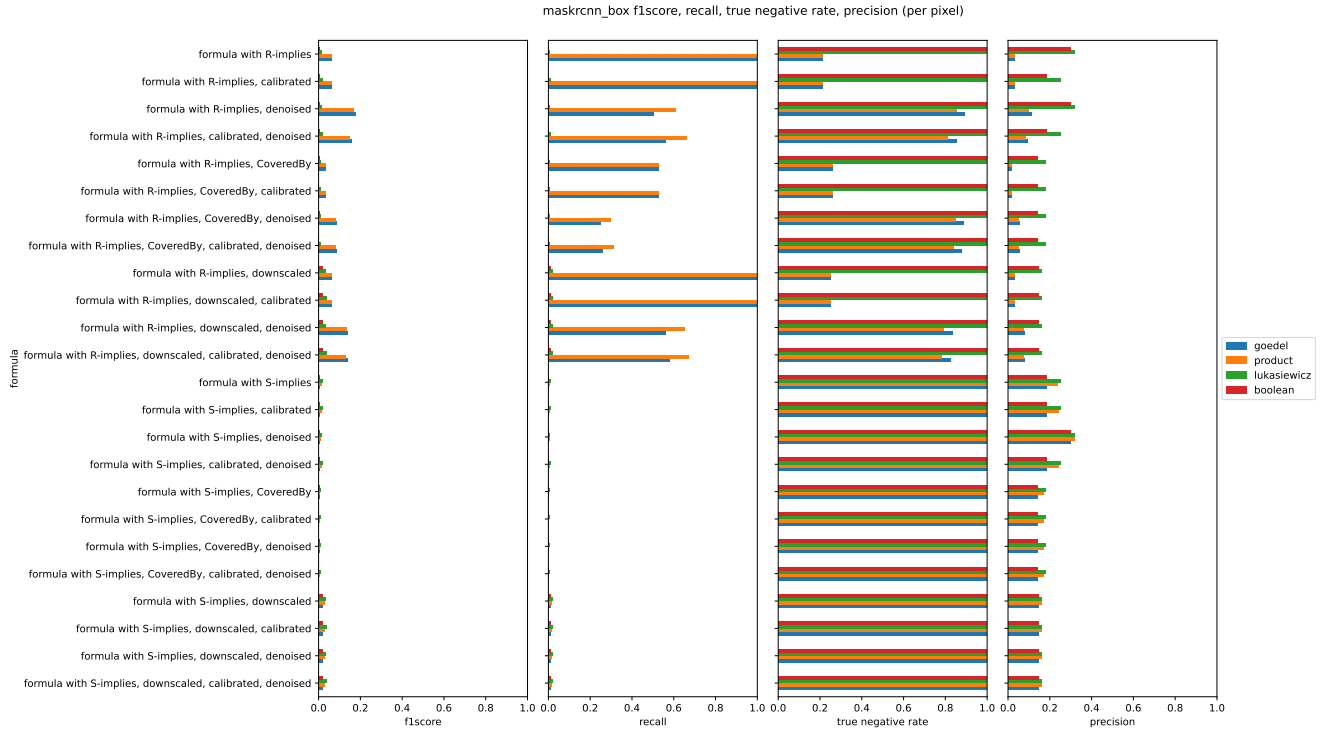


Figure 3. **Mask R-CNN, pixel-level monitor**: Visual comparison of performance metrics for different monitor formulations (cf. Tab. 8). *Left to right*: F1 score, recall, precision, and true negative rate.

The sampling rate of the plotted curves increases towards the value boundaries of $\tau_{\text{reg}}^{\text{peaks}}$. The results show:

(1) **Varying $k_{\text{size}_{\text{GT}}}$ for a fixed $k_{\text{size}_{\text{M}}}$, and the other way round, both have little influence on the performance.**

(2) **Larger $k_{\text{size}_{\text{M}}}$ have slight performance benefits for common fixed $k_{\text{size}_{\text{GT}}}$.** This may indicate a better noise robustness of larger kernel sizes. Larger kernel sizes can differentiate the quality of truth peaks in a larger range of peak sizes, boosting the influence of large interesting areas while decreasing that of small ones. Therefore, in the main paper we used the largest considered kernel size of 33, which also nicely fits typical body part proportions in the test dataset.

(3) Fuzziness shows a consistent performance benefit

(cf. precision-recall curves).

(4) Increasing $k_{\text{size}_{\text{GT}}}$ decreases the monitor precision. This is expected, as a higher $k_{\text{size}_{\text{GT}}}$ also decreases the positive rate (cf. Tab. 9).

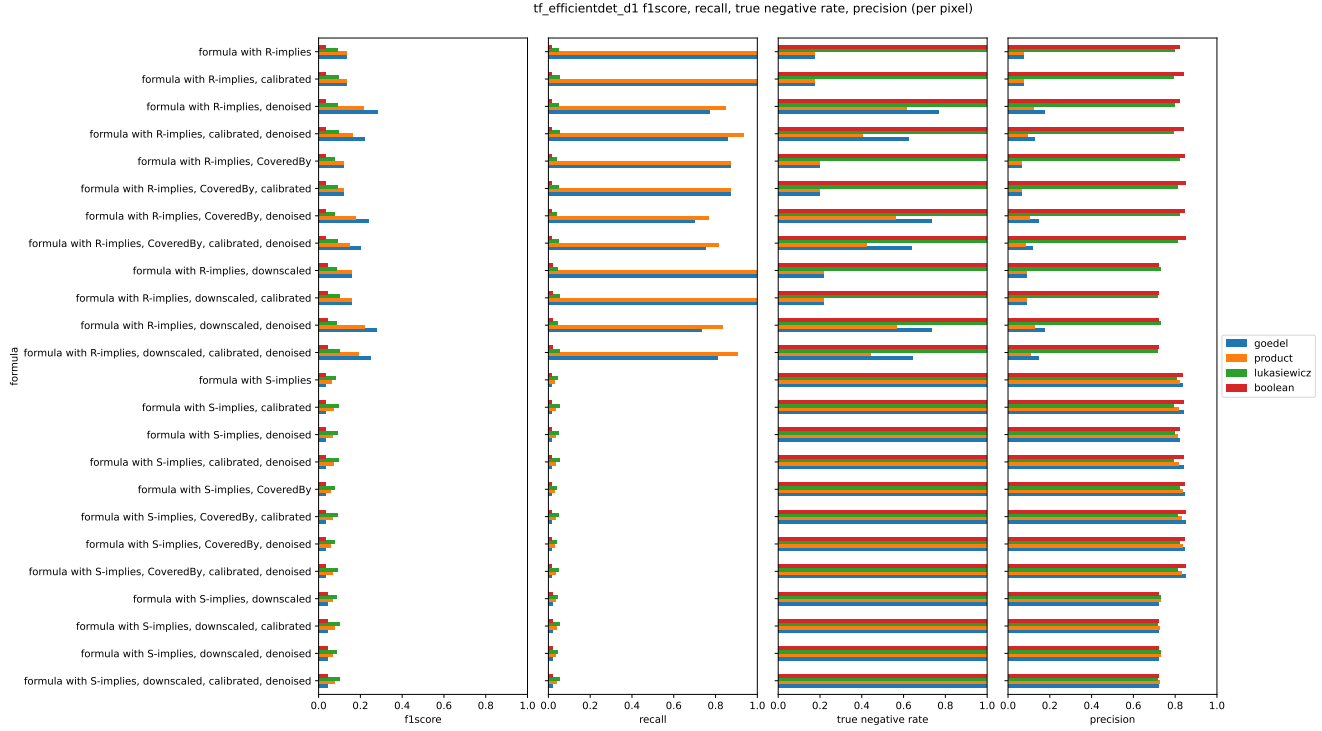


Figure 4. **EfficientDet D1, pixel-level monitor**: Visual comparison of performance metrics for different monitor formulations (cf. Tab. 8). *Left to right*: F1 score, recall, precision, and true negative rate.

k_{sizeGT}	t_{GTreg}^{peaks}	GT Pos. [%]
1	0.500	0.950
5	0.500	0.844
9	0.500	0.703
9	0.700	0.599
17	0.500	0.491
33	0.500	0.277

Table 9. Percentage of the 2693 MS COCO val2017 images with positive image-level ground truth annotations $\underline{G}_{\perp reg}^{peaks}$ for different choices of k_{sizeGT} and t_{GTreg}^{peaks} .

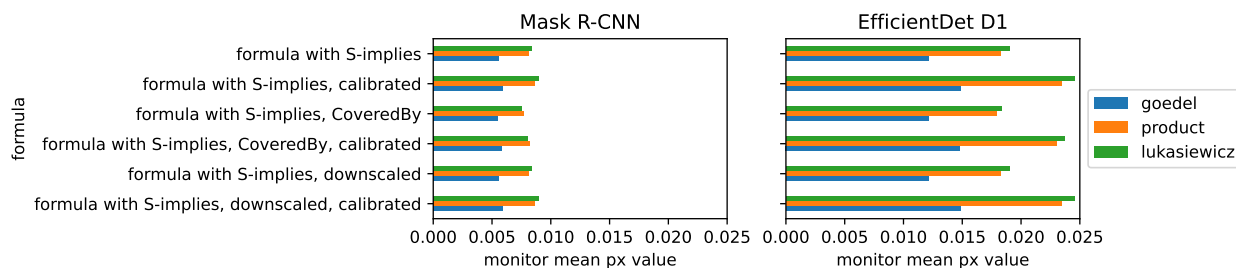


Figure 7. Comparison of values of $(1 - \text{global score})$ for different monitor formulations. This calculates as the mean of the pixel-wise monitor values over the complete dataset.

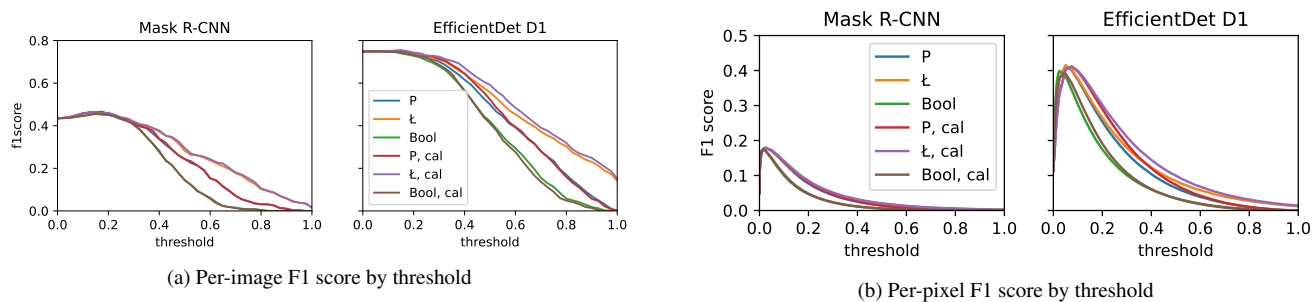


Figure 8. F1 score by $\tau_{\text{reg}}^{\text{peaks}}$ (image-level, Fig. 8a) and τ_{px} (pixel-level, Fig. 8b) for the versions of the simple rule formulations compared in the main paper.

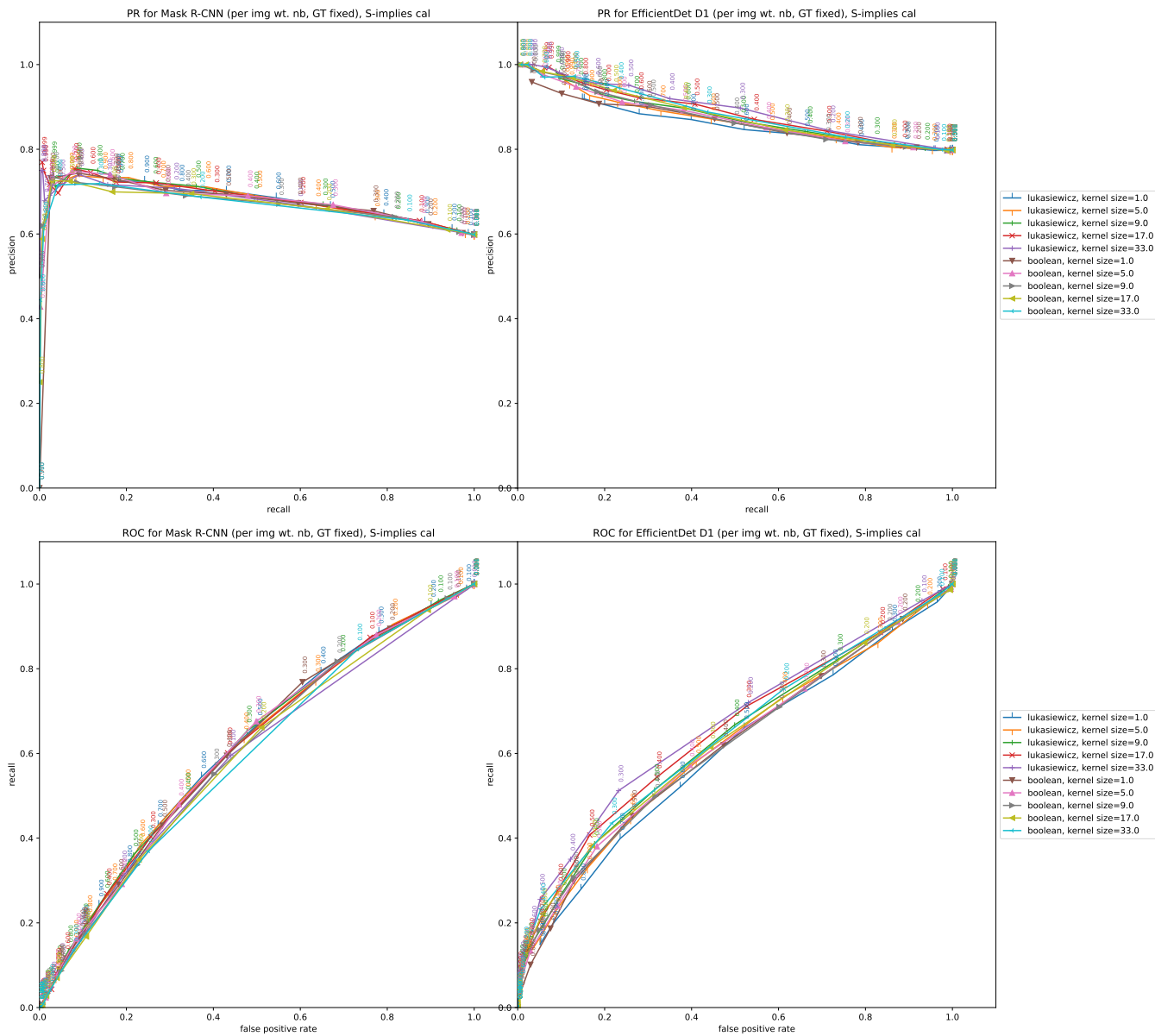


Figure 9. Results for fixed $k_{size_{GT}} = 9$ and $t_{GT_{reg}}^{peaks} = 0.7$. *Top*: Precision-recall curves, *bottom*: ROC curves over t_{reg}^{peaks} , *left*: Mask R-CNN, *right*: EfficientDet D1.

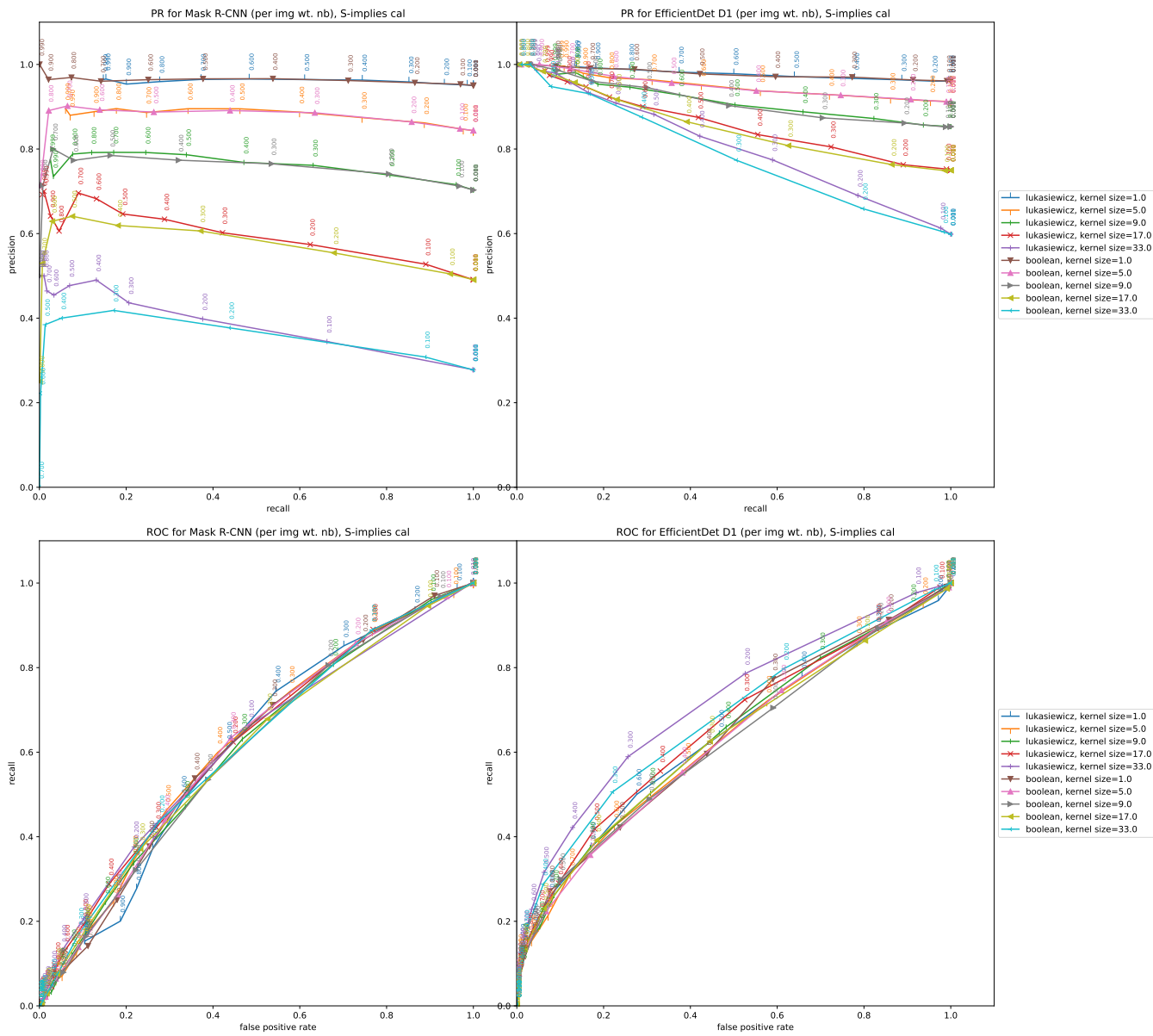


Figure 10. Results for $ksize_M = ksize_{GT}$ and $t_{Reg}^{peaks} = 0.5$. *Top*: Precision-recall curves, *bottom*: ROC curves over t_{Reg}^{peaks} , *left*: Mask R-CNN, *right*: EfficientDet D1.

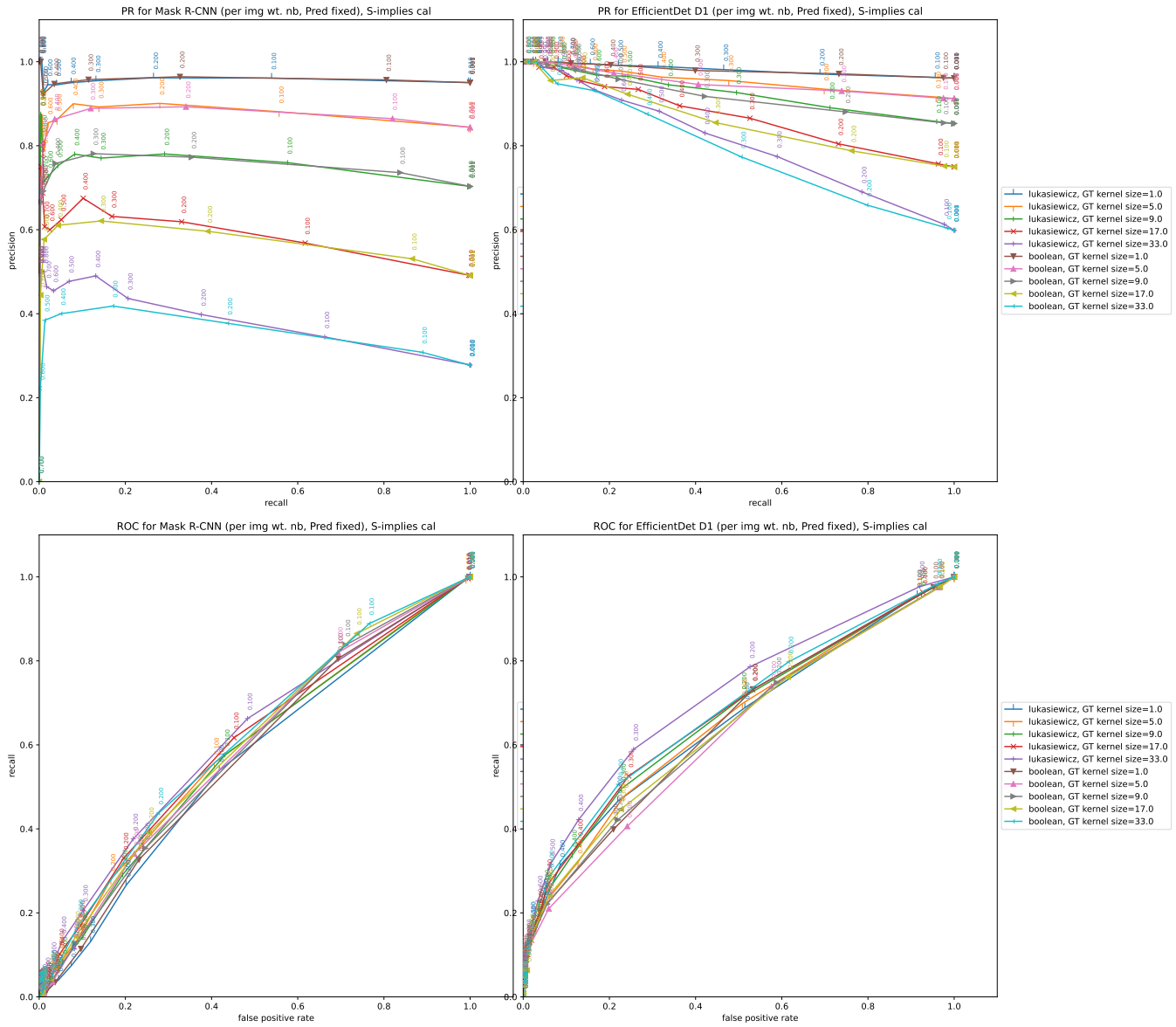


Figure 11. Results for fixed $k_{size_M} = 33$ and $t_{GTreg}^{peaks} = 0.5$. *Top*: Precision-recall curves, *bottom*: ROC curves over t_{reg}^{peaks} , *left*: Mask R-CNN, *right*: EfficientDet D1.